Symmetry Breaking and Electrical Frustration during Tip-Induced Polarization Switching in the Nonpolar Cut of Lithium Niobate Single Crystals

Anton V. Ievlev,[*,†,‡] Denis O. Alikin,[§] Anna N. Morozovska,[⊥] Olexander V. Varenyk,[∥] Eugene A. Eliseev,[#] Andrei L. Kholkin,[§,⊗] Vladimir Ya. Shur,[§] and Sergei V. Kalinin[†,‡]

[†]The Center for Nanophase Materials Sciences and [‡]Institute for Functional Imaging of Materials, Oak Ridge National Laboratory, 1 Bethel Valley Road, Oak Ridge, Tennessee 37831, United States, [§]Institute of Natural Sciences, Ural Federal University, 51 Lenin Avenue, 620000 Ekaterinburg, Russia, [⊥]Institute of Physics, National Academy of Sciences of Ukraine, 46 pr. Nauky, 03028 Kyiv, Ukraine, [∥]Taras Shevchenko Kyiv National University, 4 pr. Akademika Hlushkova, 03022 Kyiv, Ukraine, [#]Institute for Problems of Materials Science, National Academy of Sciences of Ukraine, 3 Krjijanovskogo, 03142 Kyiv, Ukraine, and [⊗]Center for Research in Ceramics and Composite Materials (CICECO) and Department of Materials and Ceramic Engineering, University of Aveiro, Aveiro 3810-193, Portugal

ABSTRACT Polarization switching in ferroelectric materials is governed by a delicate interplay between bulk polarization dynamics and screening processes at surfaces and domain walls. Here we explore the mechanism of tip-induced polarization switching at nonpolar cuts of uniaxial ferroelectrics. In this case, the in-plane component of the polarization vector switches, allowing for detailed observations of the resultant domain morphologies. We observe a surprising variability of resultant domain morphologies stemming from a fundamental instability of the formed charged domain wall and associated electric frustration. In particular, we demonstrate that controlling the vertical tip position allows the polarity of the switching to be controlled. This represents a very unusual form of symmetry breaking where mechanical motion in the vertical direction controls the lateral domain growth. The implication of these studies for ferroelectric devices and domain wall electronics are discussed.

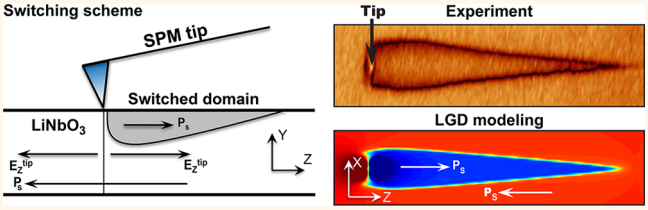

KEYWORDS: ferroelectric · domain structure · polarization switching · scanning probe microscopy · lithium niobate · symmetry breaking

Polarization reversal in ferroelectric materials underpins functionality of a broad range of optoelectronic, data storage, and computational devices.[1−4] These applications have stimulated a large number of the experimental studies as well as detailed theoretical analyses.[5−8] The classical description of polarization reversal process considers purely physical mechanisms in which the coupling between the electric field and polarization provides the driving force and the interplay between the driving force and depolarization and wall energies controls the thermodynamics of the forming domains. However, simple considerations of the electrostatic field energy suggest that external and bulk screening processes will critically affect the energies of forming nuclei and growing domains, providing nontrivial contribution to switching process.[9,10] The earlier analysis of switching using solid electrodes considered the purely electronic screening mechanisms, giving rise to the field of ferroelectric semiconductors in the 1980s.[11] However, more recent studies of scanning probe microscopy (SPM) tip-induced switching demonstrate the role of slower and thermodynamically favorable ionic processes and electrochemical reactions.[4,12] In real materials, the transition between different screening mechanisms is possible, resulting in intrinsically complex time-dependent phenomena.

Understanding the role of surface electronic and ionic screening and electrochemical phenomena becomes particularly relevant upon transition to nanoscale. Recent studies using X-ray methods have demonstrated that subtle changes in chemical potential of environment can result

* Address correspondence to ievlevav@ornl.gov.

Received for review November 3, 2014 and accepted December 15, 2014.

Published online December 15, 2014
10.1021/nn506268g

in chemically induced polarization reversal in thin films.[13−15] However, these studies allow insight only in average system behavior, while a detailed mechanism operational on the single domain level and control of the local polarization state require probe-based studies.

Switching processes under the action of a strongly inhomogeneous electric field produced by the SPM tip have been extensively studied by many scientific groups in uniaxial ferroelectrics as a model material.[16−27] However, most parts of those studies are limited by consideration of the polarization reversal on the polar cuts (spontaneous polarization is perpendicular to sample surface) and switching by vertical component of the SPM tip electric field. In this case, only one cross-section of a 3D ferroelectric domain can be visualized by PFM, and the information about the structure of domain in directions normal to the sample surface is not available. Recent investigations by Raman confocal microscopy demonstrated the possibility of domain visualization in the sample bulk;[28−30] however, spatial resolution is limited by a few hundred nanometers, which is not enough for the visualization of domain features at the nanometer scale. Normal polarization switching is associated with changes in surface polarization bound charge which can naturally be compensated by the electronic charge injection from the tip and surface electrochemical reactions that dominate intrinsic materials response.

SPM investigations on nonpolar cuts (spontaneous polarization is in the surface plane) provide suitable alternatives. The existence of lateral components of electric field produced by the tip allows switching process and lateral PFM mode[31] allows visualization of resulted domains with nanometer spatial resolution. Tip-induced polarization switching on the nonpolar cuts has been recently theoretically considered in terms of equilibrium thermodynamic approach in lithium niobate and lithium tantalate single crystals[27,32] and experimentally studied in relaxor strontium barium niobate.[33] We note that studies of in-plane polarization switching can be of interest in multiple aspects. First of all, these can be expected to provide cross-sectional studies of the domain geometry, including parameters such as intrinsic domain shape, opening angle, and kinetics of forward and sideways growth. Second, both domain walls will necessarily be charged, allowing fundamental insight both into stability and electronic properties of strongly charged domain walls and potential applications in domain wall electronic devices. Finally, time evolution of these systems can provide information on driving forces and bulk screening mechanism in bulk materials.

Here we systematically studied formation and growth of isolated domains on the surface of the nonpolar cut of lithium niobate single crystal. While in certain cases a formation of theoretically predicted wedge type domains was observed, in many cases we observed formation of complex interlocked wedge-type shapes and complex domain geometries. Polarization reversal kinetics was found to be crucially dependent on the polarity of applied switching pulses. We attribute this surprising variability of the domain morphologies to a combination of phenomena (motion of the charged domain walls, charge injection, and screening) producing a strongly inhomogeneous electric field. Furthermore, we demonstrate that controlling the vertical tip position allows the polarity of the switching to be controlled. This represents very unusual form of symmetry breaking where mechanical motion in vertical direction controls the domain growth in lateral direction. Theoretical calculations and computer simulations using the Landau−Ginzburg−Devonshire model allowed us to describe the kinetics of formation and growth of the wedge-shaped domain and showed good agreement with experiments. The obtained results are important for further understanding of the polarization switching processes in ferroelectric materials and their practical applications.

RESULTS

The process of polarization reversal on nonpolar cuts of uniaxial ferroelectric is different from the switching on polar cuts both in terms of driving force and effects of depolarization fields. The main driving force of the switching in this case is the lateral component of tip-induced electric field directed against spontaneous polarization. Therefore, morphology of formed domains is defined by spatial distribution of this field. In the case of polar cut, the vertical component of the electric field reaches its maximum under the tip and decreases with distance.[34] This determines symmetric with respect to SPM tip position shape of resulted domains.[18,19] Distribution of lateral component of electric field produced by the tip in terms of point charge model can be calculated using potential from ref 32

$$E_Z(x,y,z) = \frac{U_{sw}C_{tip}}{2\pi\varepsilon_0(\sqrt{\varepsilon_{11}\varepsilon_{33}}+1)}\frac{z}{(z^2+\gamma^2x^2+(R_{tip}+\gamma y)^2)^{3/2}} \quad (1)$$

where U_{sw}, C_{tip}, and R_{tip} are the tip bias, capacitance, and curvature radius, respectively, ε_{11} and ε_{33} are the dielectric constants along nonpolar and polar directions, respectively, and $\gamma = (\varepsilon_{33})/(\varepsilon_{11})^{1/2}$ is the anisotropy constant.

Calculations showed that the z-component of the electric field is equal to zero under the tip and has a maximum at a distance close to tip radius (Figure 1). Such field distribution leads to nontrivial kinetics of the polarization reversal process. Domain growth is possible along one direction of the polar axis, where the electric field is directed against spontaneous polarization (Figure 1c,d). Changing of the bias sign reverse direction of electric field produced by the tip and should change the direction of the domain growth. At the same time, switching is impossible in the area right under the tip.

However, experiments demonstrated switching dynamics (Figure 2a) completely different from simple

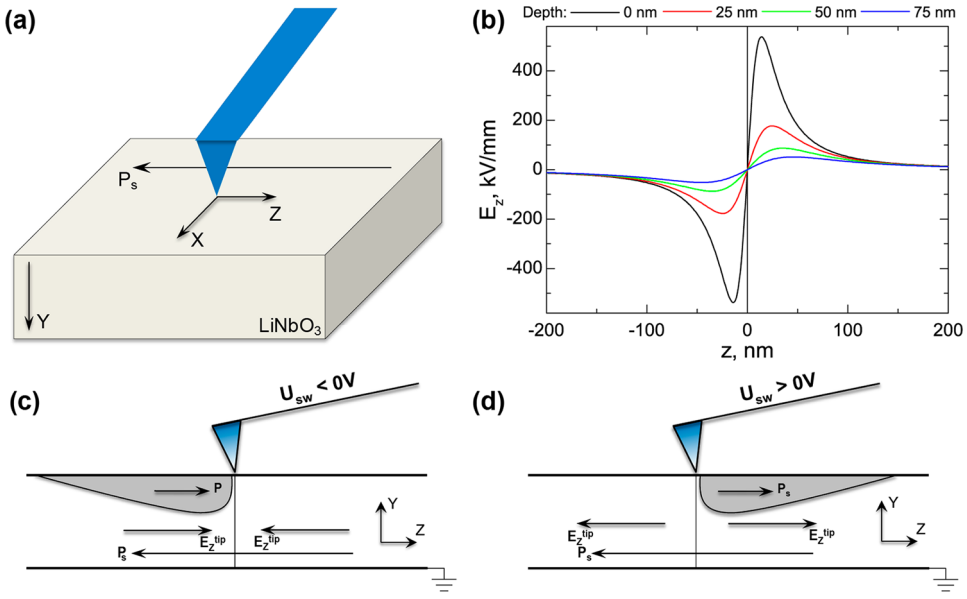

Figure 1. (a) Schematics of experiment and coordinate system used in calculations. (b) Distribution of *Z*-component of electric field produced by the tip along line $x = 0$ on the sample surface and different depths in the bulk. (c, d) Expected domain configuration in the case of negative and positive bias, respectively.

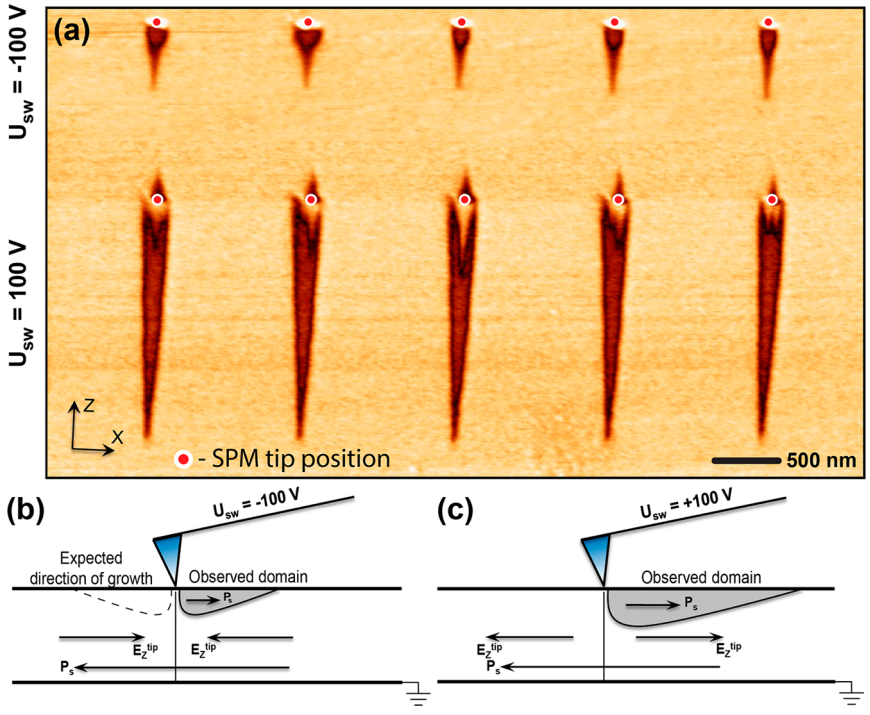

Figure 2. (a) PFM-amplitude images of domains formed after switching on Y-cut of lithium niobate singe crystal by single rectangular pulses with amplitude $U_{sw} = \pm 100$ V and duration $t_{sw} = 1$ s applied to the SPM tip. (b, c) Switching schemes for negative and positive switching pulses, respectively.

theoretical expectations. Both negative and positive pulses led to formation of wedgelike domains in the same direction (with respect to the *x*-axis). Switching by positive pulses (Figure 2c) led to formation of relatively long (1.5−2 μm) domains in the "right" direction (electric field directed against spontaneous polarization). Small distortions of the domain shape and short domains in the opposite direction will be discussed below. Unexpected switching by negative pulses led to formation of shorter domains (500−750 nm) in the "wrong" direction (*i.e.*, the same as for positive bias but against the field in this case). This phenomenon cannot be explained in terms of classic domain nucleation and growth because electric filed in that area has the same direction with spontaneous polarization (Figure 2b).

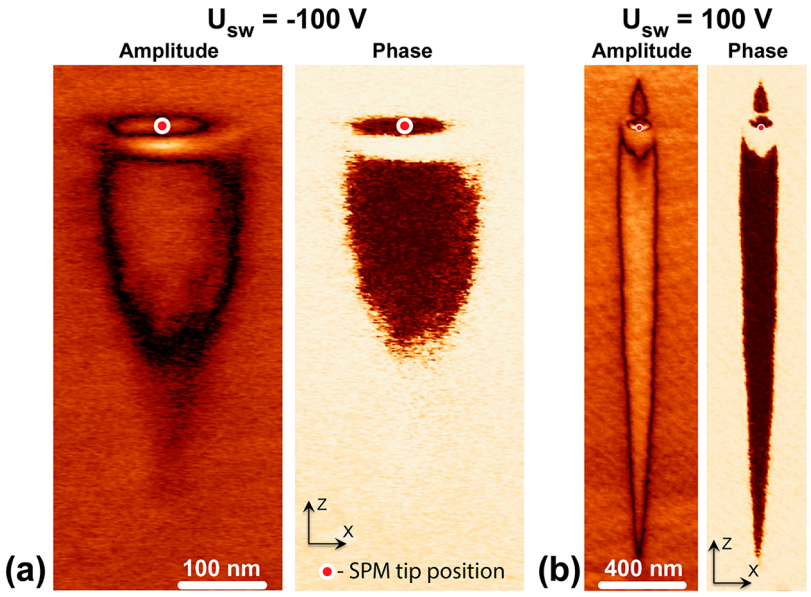

Figure 3. Detailed PFM images of the domains on Y-cut of lithium niobate single crystal. Switching by (a) negative and (b) positive single rectangular pulses.

Detailed PFM images reveal additional details in the domain morphologies (Figure 3), namely formation of complex interlocked domains at the domain base. In the case of negative pulse (Figure 3a), in addition to the main wedgelike domain there was a small elliptical domain under the tip and area with enhanced piezoresponse between these two domains. Visualization of the domains formed after switching by positive pulses demonstrated an even more complicated structure (Figure 3b). In addition to the long wedgelike domain and elliptical domain under the tip short (200−250 nm), wedgelike domain in opposite direction can be observed. In addition, the main domain displayed a pronounced backswitched area with the nested domain in the initial polarization direction

Observed domain morphologies are significantly different from the shapes predicted using an equilibrium thermodynamic approach.[32] This fact can be attributed to the interplay between the charged domain wall and screening processes on the sample surface and in the sample bulk, leading to sequence of complex morphological transformations controlled by kinetics of associated processes. Due to the inherent spatial and dynamic complexity of the system, not all of these phenomena can be addressed theoretically. Therefore, the logic of the study is constructed in the following way. First, we consider an idealized thermodynamic domain growth and then qualitatively describe the contributions of phenomena not amenable to direct modeling. Finally, we discuss the implication for domain switching studies and opportunities for domain structure control based on explored phenomena.

Kinetics of the Wedge-Shaped Domain Growth. To model the process of the domain formation and growth we used Landau−Ginzburg−Devonshir (LGD) theory.[35] We considered a two-layered system formed by an air layer and ferroelectric of thickness L, separated by surface $y = 0$. Ferroelectric polarization distribution directed along z-axes, $P_z(x,y,z)$, satisfies the dimensionless LGD equation in the ferroelectric region, at $-L < y < 0$:

$$\frac{\partial \tilde{P}_z}{\partial \tau} - \tilde{P}_z + \tilde{P}_z^3 - R_c^2\left(\frac{\partial^2 \tilde{P}_z}{\partial z^2} + \frac{\partial^2 \tilde{P}_z}{\partial y^2} + \frac{\partial^2 \tilde{P}_z}{\partial x^2}\right) = \tilde{E}_z \quad (2)$$

Here, $\tilde{P}_z = P_z/P_s$ is ferroelectric polarization normalized on the spontaneous polarization $P_S = 0.75$ C/m^2, and the external field $\tilde{E}_z = E_z/E_c$ is normalized on the coercive field that value $E_c = 5 \times 10^7$ V/m was taken from the best fitting to experimental data.

Dimensionless time τ is introduced as $\tau = t/\tau_0$, where characteristic time $\tau_0 = -\Gamma/\alpha$ is determined by the ratio of kinetic Khalatnikov coefficient Γ and generalized dielectric stiffness $\alpha = \alpha_T(T - T_C)$, correlation length $R_c = (-g/\alpha)^{1/2}$ is about 1 nm at room temperature and g is the gradient coefficient in the LGD potential. We considered case of perfectly screened ferroelectric, which was provided by boundary charges with surface density σ on polar surfaces, $\sigma(z = \pm W) = \pm P_s$, where $2W$ − size of the model in z direction. Equation 2 also should be supplemented by the boundary conditions far from the probe apex $\tilde{P}_z(x,z \to \infty) = \pm 1$ (and naturally $\partial \tilde{P}_z/\partial x_i \to 0$).

To define quasistationary electric field E_z in eq 2, the corresponding potential φ can be introduced as $E = -\nabla\varphi$. The potential φ satisfies electrostatic equations inside the layered system, namely the Laplace equation, $((\partial^2/\partial z^2) + (\partial^2/\partial y^2) + (\partial^2/\partial x^2)\varphi_d = 0$, inside the air/vacuum ambient semi space, $0 < y < +\infty$ (excluding tip volume). The equipotential surface corresponds to the biased conductive tip surface, $\varphi_d|_{tip} = U$. The tip apex was regarded spherical with small flat contact

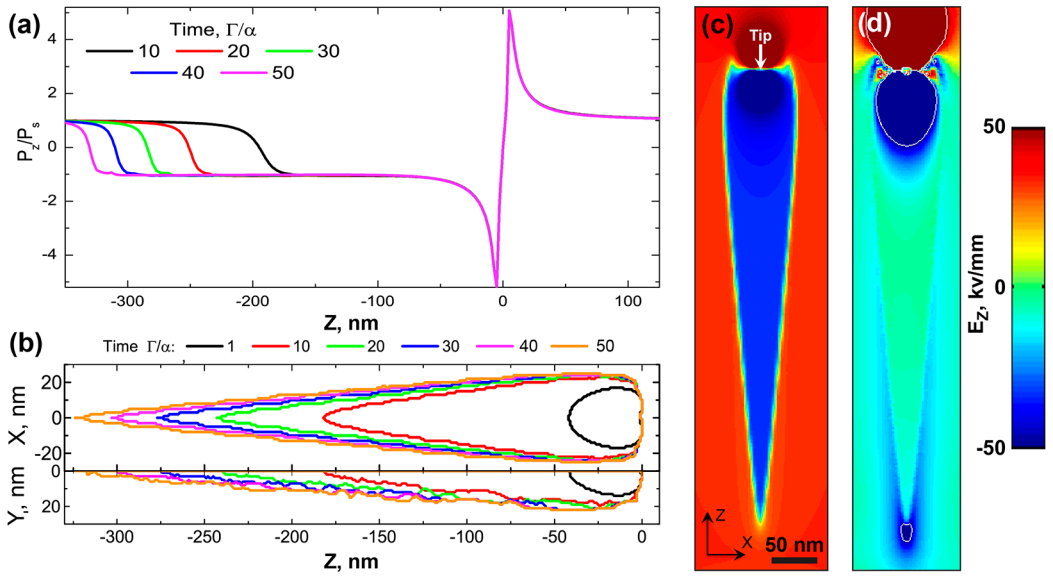

Figure 4. LGD simulation of the domain growth under SPM probe on LNO Y-cut. (a) Polarization profiles across LNO-surface *z*-line at different time moments indicated at the layer on the plot. (b) Evolution of the domain shape (*x*−*z* and *y*−*z* cross sections). Contour maps of polarization P_z (c) and electric field E_z (d) across the *x*−*z* plane (*y* = 0 nm) at the time moment $t = 50\tau_0$.

plate, placed in a physical point contact with ferroelectric surface. The boundary conditions at the interface $y = 0$ are continuous potential on the boundaries between ferroelectric layer and ambient, $\varphi_f(x,y = 0,z) = \varphi_d(x,y = 0,z)$, and continuous normal component of displacement, $D_y^d - D_y^f|_{y=0} = 0$, where $D_y^f = \varepsilon_0\varepsilon_{11}^f(\partial\varphi_f/\partial y)$ and $D_y^d = \varepsilon_0\varepsilon_{11}^d(\partial\varphi_d/\partial y)$. Maxwell equation div$D = 0$ along with the definition, $D_{x,y} = \varepsilon_0\varepsilon_{11}^f E_{x,y}$ and $D_z = \varepsilon 0E_z + P_z^{\text{total}} \approx \varepsilon_0\varepsilon_{33}^b E_z + P_z^{\text{FE}}$, yields to anisotropic Poisson relationship inside ferroelectric-semiconductor layer $-L < y < 0$. Including polarization gradient, potential distribution within ferroelectric is

$$\varepsilon_0\left(\varepsilon_{33}^b\frac{\partial^2\varphi_f}{\partial z^2} + \varepsilon_{11}^f\left(\frac{\partial^2\varphi_f}{\partial x^2} + \frac{\partial^2\varphi_f}{\partial y^2}\right)\right) = \frac{\partial P_z}{\partial z} \quad (3)$$

Here, $\varepsilon_0 = 8.85 \times 10^{-12}$ F/m is the universal dielectric constant, $\varepsilon_{33}^b \approx 5$ is the background dielectric permittivity of the ferroelectric, and $\varepsilon_{11}^f = 84$. The grounded bottom electrode was considered by the zero potential boundary condition, $\varphi_f(x,y = L,z) = 0$.

Using the COMSOL Multiphysics package, we considered the cases of domain formation with the (a) presence and (b) absence of the free charge carriers in the Debye approximation. The SPM tip was modeled by part of the sphere with radius $R_{\text{tip}} = 25$ nm and conical part with angle 10°, oriented normally to the sample surface.

We found that inclusion of the carriers in conventional form and for realistic concentrations (10^{23}–10^{25} m^{-3}) does not provide any significant changes in the distribution of the potential and polarization across the domain. Introduction of the charge carries should lead to the appearance of the screening; however, in our case the screening effect would make visible changes only if the value of density of the charge carriers is comparable to the polarization gradient $\partial P_z/\partial z$ value, which can be roughly estimated as10^9C/m^3. According to this estimation, the charge density in turn should be approximately equal to 10^{28} 1/m^3, which is close to a half-metal. However, this fact can be explained by the limitations of the used Debye model. Taking into account of the nonlinear screening processes potentially can change simulation results.

Results of the COMSOL finite element simulations *in the dielectric limit* with the absence of charge carriers are presented in Figure 4. In simulation we used tip radius 20 nm, tip bias $U_{\text{sw}} = +100$ V. Time evolution of the domain shape can be found in the supplementary video file and in Figure 4a,b.

The calculated spatial distribution of polarization (Figure 4a) has two components: spontaneous and induced. Spontaneous polarization ($\tilde{P} = \pm 1$) far from the tip has completely ferroelectric origin, while electric field induced component leads to the appearance of polarization peaks near the tip.

Simulated domains at late growth stages (Figure 4b,c) demonstrate well-defined wedgelike shape and in a good agreement with experimental results (Figure 3). One should note that this shape is far from semiellipsoidal as used by Pertsev and Kholkin[32] in an equilibrium thermodynamic approach. Calculation of spatial distribution of electric field near the charged domain wall of the growing domain (Figure 4d) confirms the existence of a breakdown effect predicted in (ref 36) and explains domain growth in the areas with external electric field well below the coercive one. Breakdown is caused by the spatial distribution of the electric field in the immediate vicinity of the domain apex. Simulations show

that sign and value of the electric field produced by charged domain walls supports forward domain growth even in the areas where the tip field is already faint. This leads to reaching the submicron and even micron domain lengths. The domain breakdown effect has been recently experimentally observed in $LiNbO_3$ for a different geometry.[37] The detailed numerical analysis of the domain growth and breakdown phenomenon for nonpolar cuts will be published elsewhere.

Characteristics Features of the Domain Shapes. The experimentally observed overall wedgelike shape of the domains is consistent with simulated data (Figure 4). However, experiments demonstrated both the presence of more complex domain morphologies and finer details in the wedge domains. All the observed characteristic features of the domain shape can be divided into a few groups: (1) backswitching with formation of the domain in the "wrong" direction (Figure 3b); (2) formation of the isolated domain under the tip (Figure 3a); (3) presence of the area with enhanced piezoresponse near the tip (Figure 3a). We will discuss these phenomena in details below.

The presence of a partially backswitched area on the domains formed after application of positive pulse leads to consideration of a dual-stage switching process, including tip-induced switching and backswitching stages. Polarization reversal under the action of tip-induced electric field leads to formation of a long prolate domain in the first stage; backswitching on the second stage leads to partial restoration of initial polarization inside the domain and formation of short domain in the opposite direction. Similar behavior on polar cuts of ferroelectrics with formation of the doughnut-shaped domains was reported recently in the number of studies.[12,24,38−40] This phenomenon can be explained using the same approach. External electric field in a considered configuration is concentrated in a small area under the tip and leads to a redistribution of charge carriers on the sample surface and into the bulk (screening of the SPM tip field). When bias is switched off these charges produce an electric field with opposite direction to external electric field.

However, spatial distribution of the electric field component along polar axis E_z in the current experimental configuration differs significantly from the polar one (Figure 1b). Backswitching in this case has two pronounced contributions (Figure 3b): well-known restoration of the initial polarization direction inside the main wedge domain (analogue of the formation of doughnut-shaped domains on the polar cut) and growth of the new wedge-shaped domain in the opposite direction. The morphology of the domain structures formed on the second stage (symmetric growth in both direction with respect to the tip position) demonstrates that charges caused the second switching stage are located exactly under the tip.

The morphology of the resulted domain structures is controlled by efficiency and the time dynamics of the backswitching stage. This explains anomalous direction of the domain growth observed for negative bias (Figure 3a). In this case, backswitching leads to complete disappearing of the initial domain, and consequent PFM visualization reveals the domain formed on the second switching stage (with opposite direction).

Pronounced anisotropy of the backswitching stage can be attributed to anisotropy of the charge carriers (ions) existing in the top adsorption layer. The recently environmental studies demonstrated a number of phenomena which were attributed to screening process by ions in the thin surface water layer.[4,12] In addition, time-resolved Kelvin probe force microscopy measurements demonstrated higher value of the mobility of the negative ions (in comparison with positive ions) on the surface of lithium niobate single crystal.[41] This fact explains observed experimental results. Screening of the domain formed by positive pulses is faster; therefore, backswitching stage is not so pronounced, like for the negative pulses.

The second characteristic feature of the domain morphology is a presence of the small isolated domain in the area right under the tip. It can be explained as a result of spontaneous bacswitching in the area near the tip which is caused by nontrivial spatial distribution of the electric field (Figure 4d). Simulation predicts the presence of the areas ($z > 0$ nm; $x \approx \pm 20$ nm), where the z-component of electric field has direction supporting switching and a value that is high enough (above coercive field) for the switching. Such a distribution of electric field can lead to the formation of isolated domain under the tip after termination of the switching pulse.

We can assume that the third type of the characteristic features, presence of the area with enhanced piezoresponse (Figure 3a), can be caused by depolarization electric field distribution produced by charged domain walls in the sample bulk and corresponded interaction with SPM tip during visualization.

The deviations of the domain shape in proximity to the SPM tip are not surprising. The polarization switching considered in the current manuscript represent delicate interplay of various phenomena, including motion of the charged domain walls, screening by charge carriers on the sample surface and in the sample bulk, charge injection, *etc*. The main supporting factor is the fundamental instability of the charged domain wall, which cannot be completely screened with absence of the slow bulk screening processes (characteristic time up to few seconds[42]). This leads on the one hand to formion of the shallow structures to minimize electrostatic energy. On the other hand, this increases energies of the domain wall and biased tip. Competition of these two processes in the absence

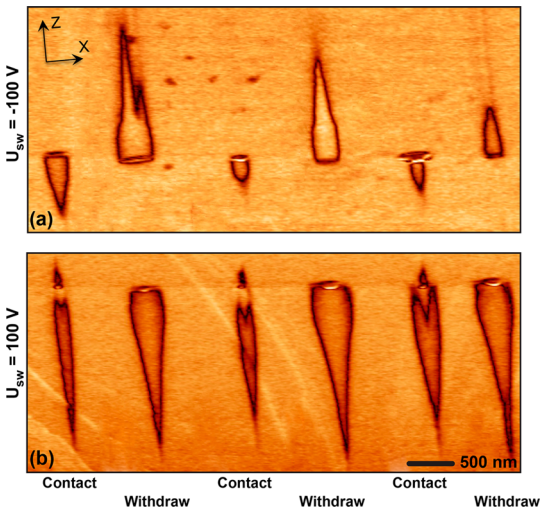

Figure 5. PFM–amplitude images of the domains formed after switching on Y-cut of lithium niobate single crystal. SPM tip stays in contact after termination of the pulse ("Contact" mode) or is withdrawn form the surface with applied bias ("Withdraw" mode) as labeled on the figure. Switching by (a) negative and (b) positive single rectangular pulses.

(inefficiency) of bulk screening leads to electrical frustration at the domain wall with formation of characteristic domain features (elliptic domain, enhanced piezoresponse) in vicinity of the tip.

Symmetry Breaking Induced by Mechanical Tip Motion. Investigated phenomena are important for the fundamental studies in the field of ferroelectric physics. Moreover, dual-stage kinetics opens opportunities of the control of domains growth direction by changing of the switching stages.

To demonstrate this, we designed experiments with controlled vertical motion of the biased SPM tip (Figure 5). In these experiments, two lines of the domains have been formed using standard switching procedure (each odd domain in the line) and procedure with withdrawing of biased tip before switching pulse ends (each even domain in the line). Obtained results demonstrated fundamental difference between domain shapes for both negative (Figure 5a) and positive (Figure 5b) pulse polarities.

The shapes of the domain observed in the withdraw mode (Figure 5) are very close to theoretical simulations (Figure 4c). This fact can be naturally explained by a dual-stage mechanism of the switching process in the contact mode. The first stage can be described by a pure LGD approach, while more complicated processes should be modeled for simulation of the second stage. Complex nontrivial distribution of electric field existed in the area under the grounded tip just after termination of the switching pulse considerably change resulted domain structure.

Observed experimental results demonstrated extremely unexpected switching behavior when vertical motion of the tip (*y*-direction) allows controlling kinetics of the domain growth along perpendicular *z*-direction. This potentially can be used for future practical applications of the ferroelectric materials as variability of the resultant domain structures can be drastically increased.

CONCLUSION

We experimentally studied the processes of tip-induced polarization reversal on a nonpolar cut of lithium niobate single crystal and revealed a formation of complex domain structures consisting of a few separate domains. We found that changing of the polarity of switching pulses does not lead to a change of the domain growth direction as expected from spatial distribution of electric field. This fact has been explained by complex kinetics of the switching process. We showed that switching proceeds in two separate stages: (1) switching during application of switching pulse and (2) "backswitching" after pulse termination. Observed strong anisotropy of the backswitching stage led to the essential differences in the morphology of domains formed by switching pulses of opposite polarities and has been attributed to different values of mobility of charge carriers on the sample surface and in the sample bulk participating in the screening of fresh domains.

Theoretical calculations in Landau–Ginzburg–Devonshire theory allowed simulating formation and growth of the wedge-shaped domains with shapes close to experiment. Moreover, calculations of electric field spatial distribution near the charged domain wall confirmed breakdown phenomenon and explained experimentally observed growth of the domains in the areas with external electric field below the coercive one.

Obtained results are important from both fundamental and practical points of view. From a fundamental point of view, this study allows us to model a process of the formation and growth of the domains with charged domain walls. Moreover, it opens opportunities for experimental and theoretical studies of poorly known process of forward domain growth in the sample bulk. From a practical point of view, we explored unusual symmetry breaking, where vertical motion of the SPM tip controls the domain growth and can potentially give a rise to development of novel techniques for domain control useful for various ferroelectric applications.

METHODS

As a model system, we used a plate of congruent $LiNbO_3$ single-crystal cut perpendicular to the *Y* (010) crystallographic direction. Lithium niobate single crystals represent good model uniaxial ferroelectric material because it has only two possible antiparallel directions of spontaneous polarization. Moreover, the industrial technique of these crystals growth provides samples with low concentrations of defects. The thickness of

the sample has been decreased by mechanical polishing down to 20 μm. Experiments were performed with a commercial scanning probe microscope Dimension 3100 (Bruker, USA). Multi-75G-E (Budget Sensors, USA) SPM tips with a conductive platinum coating and 25−35 nm of typical curvature radius have been used. Polarization reversal was carried out by application of the single rectangular pulses with amplitude U_{sw} ranging from −100 to +100 V and with duration t_{sw} = 1 s to the SPM tip. Lateral piezoresponse force microscopy has been used for visualization of resulted domains. Experiments were carried out under environmental conditions (room temperature and 30% of relative humidity).

Conflict of Interest: The authors declare no competing financial interest.

Acknowledgment. A portion of this research (A.V.I, S.V.K.) was conducted at the Center for Nanophase Materials Sciences, which is a DOE Office of Science User Facility. V.Y.S., A.L.K., and D.O.A. acknowledge CNMS user proposal, the Ministry of Education and Science of the Russian Federation (Contract No. 14.594.21.0011) and RFBR (Grant Nos. 13-02-01391-a and 14-02-90447-Ukr-a). A.N.M., O.V.V., and E.A.E. acknowledge National Academy of Sciences of Ukraine (Grant No. 35-02-14) and the Center for Nanophase Materials Sciences, user projects CNMS 2013-293 and CNMS 2014-270. The work in CICECO is partly supported by the FCT grant Pest-C/CTM/LA0011/2013.

Supporting Information Available: Movie of the LGD simulation of the tip-induced domain growth on the nonpolar Y-cut of the lithium niobate single-crystal. This material is available free of charge *via* the Internet at http://pubs.acs.org.

REFERENCES AND NOTES

1. Hatanaka, T.; Nakamura, K.; Taniuchi, T.; Ito, H.; Furukawa, Y.; Kitamura, K. Quasi-Phase-Matched Optical Parametric Oscillation with Periodically Poled Stoichiometric $LiTaO_3$. *Opt. Lett.* **2000**, *25*, 651–653.
2. Cho, Y.; Fujimoto, K.; Hiranaga, Y.; Wagatsuma, Y.; Onoe, A.; Terabe, K.; Kitamura, K. Tbit/Inch^2 Ferroelectric Data Storage Based on Scanning Nonlinear Dielectric Microscopy. *Appl. Phys. Lett.* **2002**, *81*, 4401–4403.
3. Sohler, W.; Hu, H.; Ricken, R.; Quiring, V.; Vannahme, C.; Herrmann, H.; Büchter, D.; Reza, S.; Grundkötter, W.; Orlov, S.; *et al.* Integrated Optical Devices in Lithium Niobate. *Opt. Photonics News* **2008**, *19*, 24–31.
4. Ievlev, A. V.; Jesse, S.; Morozovska, A. N.; Strelcov, E.; Eliseev, E. A.; Pershin, Y. V.; Kumar, A.; Shur, V. Y.; Kalinin, S. V. Intermittency, Quasiperiodicity and Chaos in Probe-Induced Ferroelectric Domain Switching. *Nat. Phys.* **2014**, *10*, 59–66.
5. Scott, J. F. Nanoferroelectrics: Statics and Dynamics. *J. Phys.: Condens. Matter* **2006**, *18*, R361–R386.
6. Scott, J. F. Applications of Modern Ferroelectrics. *Science* **2007**, *315*, 954–959.
7. Dawber, M.; Rabe, K. M.; Scott, J. F. Physics of Thin-Film Ferroelectric Oxides. *Rev. Mod. Phys.* **2005**, *77*, 1083–1130.
8. Tagantsev, A. K.; Gerra, G. Interface-Induced Phenomena in Polarization Response of Ferroelectric Thin Films. *J. Appl. Phys.* **2006**, *100*, 051607.
9. Krug, I.; Barrett, N.; Petraru, A.; Locatelli, A.; Mentes, T. O.; Nino, M. A.; Rahmanizadeh, K.; Bihlmayer, G.; Schneider, C. M. Extrinsic Screening of Ferroelectric Domains in $Pb(Zr_{0.48}Ti_{0.52})O_3$. *Appl. Phys. Lett.* **2010**, *97*, 222903.
10. Shur, V. Y. Kinetics of Ferroelectric Domains: Application of General Approach to $LiNbO_3$ and $LiTaO_3$. *J. Mater. Sci.* **2006**, *41*, 199–210.
11. Fridkin, V. M. *Ferroelectric Semiconductors*. (Cosultant Bureau, **1980**).
12. Ievlev, A. V., Morozovska, A. N., Eliseev, E. A., Shur, V. Y. & Kalinin, S. V. Ionic Field Effect and Memristive Phenomena in Single-Point Ferroelectric Domain Switching. *Nat. Commun. 5:4545* (**2014**).
13. Wang, R. V.; Fong, D. D.; Jiang, F.; Highland, M. J.; Fuoss, P. H.; Thompson, C.; Kolpak, A. M.; Eastman, J. A.; Streiffer, S. K.; Rappe, A. M.; *et al.* Reversible Chemical Switching of a Ferroelectric Film. *Phys. Rev. Lett.* **2009**, *102*, 047601.
14. Wang, J. L.; Pancotti, A.; Jegou, P.; Niu, G.; Gautier, B.; Mi, Y. Y.; Tortech, L.; Yin, S.; Vilquin, B.; Barrett, N. Ferroelectricity in a Quasiamorphous Ultrathin $BaTiO_3$ Film. *Phys. Rev. B* **2011**, *84*, 205426.
15. Pancotti, A.; Wang, J.; Chen, P.; Tortech, L.; Teodorescu, C.-M.; Frantzeskakis, E.; Barrett, N. X-Ray Photoelectron Diffraction Study of Relaxation and Rumpling of Ferroelectric Domains in $BaTiO_3$(001). *Phys. Rev. B* **2013**, *87*, 184116.
16. Hong, S.; Colla, E. L.; Kim, E.; Taylor, D. V.; Tagantsev, A. K.; Muralt, P.; No, K.; Setter, N. High Resolution Study of Domain Nucleation and Growth During Polarization Switching in $Pb(Zr,Ti)O_3$ Ferroelectric Thin Film Capacitors. *J. Appl. Phys.* **1999**, *86*, 607–613.
17. Paruch, P.; Tybell, T.; Triscone, J. M. Nanoscale Control of Ferroelectric Polarization and Domain Size in Epitaxial $Pb(Zr_{0.2}Ti_{0.8})O_3$ Thin Films. *Appl. Phys. Lett.* **2001**, *79*, 530–532.
18. Terabe, K.; Nakamura, M.; Takekawa, S.; Kitamura, K.; Higuchi, S.; Gotoh, Y.; Cho, Y. Microscale to Nanoscale Ferroelectric Domain and Surface Engineering of a near-Stoichiometric $LiNbO_3$ Crystal. *Appl. Phys. Lett.* **2003**, *82*, 433–435.
19. Rodriguez, B. J.; Nemanich, R. J.; Kingon, A.; Gruverman, A.; Kalinin, S. V.; Terabe, K.; Liu, X. Y.; Kitamura, K. Domain Growth Kinetics in Lithium Niobate Single Crystals Studied by Piezoresponse Force Microscopy. *Appl. Phys. Lett.* **2005**, *86*, 012906.
20. Agronin, A.; Molotskii, M.; Rosenwaks, Y.; Rosenman, G.; Rodriguez, B. J.; Kingon, A. I.; Gruverman, A. Dynamics of Ferroelectric Domain Growth in the Field of Atomic Force Microscope. *J. Appl. Phys.* **2006**, *99*, 104102.
21. Kan, Y.; Lu, X.; Wu, X.; Zhu, J. Domain Reversal and Relaxation in $LiNbO_3$ Single Crystals Studied by Piezoresponse Force Microscope. *Appl. Phys. Lett.* **2006**, *89*, 262907.
22. Liu, X.; Kitamura, K.; Terabe, K. Thermal Stability of $LiTaO_3$ Domains Engineered by Scanning Force Microscopy. *Appl. Phys. Lett.* **2006**, *89*, 142906.
23. Dahan, D.; Molotskii, M.; Rosenman, G.; Rosenwaks, Y. Ferroelectric Domain Inversion: The Role of Humidity. *Appl. Phys. Lett.* **2006**, *89*, 152902.
24. Kholkin, A. L.; Bdikin, I. K.; Shvartsman, V. V.; Pertsev, N. A. Anomalous Polarization Inversion in Ferroelectrics *via* Scanning Force Microscopy. *Nanotechnology* **2007**, *18*, 095502.
25. Pertsev, N. A.; Petraru, A.; Kohlstedt, H.; Waser, R.; Bdikin, I. K.; Kiselev, D.; Kholkin, A. L. Dynamics of Ferroelectric Nanodomains in $BaTiO_3$ Epitaxial Thin Films *via* Piezoresponse Force Microscopy. *Nanotechnology* **2008**, *19*, 375703.
26. Shur, V. Y.; Ievlev, A. V.; Nikolaeva, E. V.; Shishkin, E. I.; Neradovskiy, M. M. Influence of Adsorbed Surface Layer on Domain Growth in the Field Produced by Conductive Tip of Scanning Probe Microscope in Lithium Niobate. *J. Appl. Phys.* **2011**, *110*, 052017.
27. Ievlev, A. V.; Morozovska, A. N.; Shur, V. Y.; Kalinin, S. V. Humidity Effects on Tip-Induced Polarization Switching in Lithium Niobate. *Appl. Phys. Lett.* **2014**, *104*, 092908.
28. Shur, V. Y.; Zelenovskiy, P. S.; Nebogatikov, M. S.; Alikin, D. O.; Sarmanova, M. F.; Ievlev, A. V.; Mingaliev, E. A.; Kuznetsov, D. K. Investigation of the Nanodomain Structure Formation by Piezoelectric Force Microscopy and Raman Confocal Microscopy in Linbo3 and Litao3 Crystals. *J. Appl. Phys.* **2011**, *110*, 052013.
29. Zelenovskiy, P. S.; Shikhova, V. A.; Ievlev, A. V.; Neradovskiy, M. M.; Shur, V. Y. Micro-Raman Visualization of Domain Structure in Strontium Barium Niobate Single Crystals. *Ferroelectrics* **2012**, *439*, 33–39.
30. Shur, V. Y.; Zelenovskiy, P. S. Micro- and Nanodomain Imaging in Uniaxial Ferroelectrics: Joint Application of Optical, Confocal Raman, and Piezoelectric Force Microscopy. *J. Appl. Phys.* **2014**, *116*, 066802.

31. Eng, L. M.; Güntherodt, H.-J.; Schneider, G. A.; Köpke, U.; Muñoz Saldaña, J. Nanoscale Reconstruction of Surface Crystallography from Three-Dimensional Polarization Distribution in Ferroelectric Barium−Titanate Ceramics. *Appl. Phys. Lett.* **1999**, *74*, 233–235.
32. Pertsev, N. A.; Kholkin, A. L. Subsurface Nanodomains with in-Plane Polarization in Uniaxial Ferroelectrics *via* Scanning Force Microscopy. *Phys. Rev. B* **2013**, *88*, 174109.
33. Volk, T. R.; Gainutdinov, R. V.; Bodnarchuk, Y. V.; Ivleva, L. I. Creation of Domains and Domain Patterns on the Nonpolar Surface of $Sr_xBa_{1-x}Nb_2O_6$ Crystals by Atomic Force Microscopy. *JETP Lett.* **2013**, *97*, 483–489.
34. Rosenman, G.; Urenski, P.; Agronin, A.; Rosenwaks, Y.; Molotskii, M. Submicron Ferroelectric Domain Structures Tailored by High-Voltage Scanning Probe Microscopy. *Appl. Phys. Lett.* **2003**, *82*, 103–105.
35. Morozovska, A. N.; Eliseev, E. A.; Bravina, S. L.; Kalinin, S. V. Landau-Ginzburg-Devonshire Theory for Electromechanical Hysteresis Loop Formation in Piezoresponse Force Microscopy of Thin Films. *J. Appl. Phys.* **2011**, *110*, 052011.
36. Morozovska, A. N.; Eliseev, E. A.; Li, Y.; Svechnikov, S. V.; Maksymovych, P.; Shur, V. Y.; Gopalan, V.; Chen, L.-Q.; Kalinin, S. V. Thermodynamics of Nanodomain Formation and Breakdown in Scanning Probe Microscopy: Landau-Ginzburg-Devonshire Approach. *Phys. Rev. B* **2009**, *80*, 214110.
37. Molotskii, M.; Agronin, A.; Urenski, P.; Shvebelman, M.; Rosenman, G.; Rosenwaks, Y. Ferroelectric Domain Breakdown. *Phys. Rev. Lett.* **2003**, *90*, 107601.
38. Bühlmann, S.; Colla, E.; Muralt, P. Polarization Reversal Due to Charge Injection in Ferroelectric Films. *Phys. Rev. B* **2005**, *72*, 214120.
39. Shishkin, E. I.; Shur, V. Y.; Mieth, O.; Eng, L. M.; Galambos, L. L.; Miles, R. O. Kinetics of the Local Polarization Switching in Stoichiometric $LiTaO_3$ under Electric Field Applied Using the Tip of Scanning Probe Microscope. *Ferroelectrics* **2006**, *340*, 129–136.
40. Lilienblum, M.; Soergel, E. Anomalous Domain Inversion in $LiNbO_3$ Single Crystals Investigated by Scanning Probe Microscopy. *J. Appl. Phys.* **2011**, *110*, 052018.
41. Strelcov, E.; Ievlev, A. V.; Jesse, S.; Kravchenko, I. I.; Shur, V. Y.; Kalinin, S. V. Direct Probing of Charge Injection and Polarization-Controlled Ionic Mobility on Ferroelectric Linbo3 Surfaces. *Adv. Mater.* **2014**, *26*, 958–963.
42. Shur, V. Y.; Akhmatkhanov, A. R.; Chuvakova, M. A.; Baturin, I. S. Polarization Reversal and Domain Kinetics in Magnesium Doped Stoichiometric Lithium Tantalate. *Appl. Phys. Lett.* **2014**, *105*, 152905.